

Impact parameter dependence of incomplete fusion between 10 and 20 MeV/nucleon

E. A. Bakum, P. Decowski,* K. A. Griffioen,[†] R. J. Meijer,[‡] and R. Kamermans
R. J. Van de Graaff Laboratorium, University of Utrecht, 3508 TA Utrecht, The Netherlands
 (Received 22 December 1988)

Incomplete fusion reactions have been studied for the system $^{20}\text{Ne} + ^{27}\text{Al}$ at 10.8, 14.7, and 19.2 MeV/nucleon by measuring correlations between evaporation residues and α -particles. The exclusive evaporation residue mass distribution can be explained in a breakup fusion model where preequilibrium emission of one α -particle occurs. Complete fusion and incomplete fusion compete over a wide range of impact parameters in the entrance channel.

The understanding of the reaction dynamics for central collisions at projectile energies close to Fermi energy is important for determining the conditions that govern the production of highly excited nuclei. At beam energies between 10 and 20 MeV/nucleon, a dominating reaction process is incomplete fusion (ICF), in which a part of the excitation energy and angular momentum is removed by the forward emission of fast light particles prior to fusion.^{1,2}

The first systematic studies of single heavy-residue velocity spectra were performed by Morgenstern and co-workers^{3,4} for $^{20}\text{Ne} + ^{27}\text{Al}$ in the energy range between 3 and 20 MeV/nucleon. They observed evaporation residues (ER's) originating from fusionlike reactions with incomplete momentum transfer and determined the cross sections for complete fusion (CF) and ICF from the resulting velocity deficit. In exclusive experiments the ICF process can be selected by the measurement of ER's in coincidence with fast light particles. The multiplicities of nucleons and α particles from preequilibrium emission are about equal^{1,2} and thus most of the angular momentum is dissipated by the (heavier) α -particles. In this Rapid Communication we derive the impact parameter range for ICF reactions in the system $^{20}\text{Ne} + ^{27}\text{Al}$ from the yield of ER's correlated with fast α -particles.

Targets of ^{27}Al (thicknesses of 360–570 $\mu\text{g}/\text{cm}^2$) were bombarded with ^{20}Ne ions accelerated by the Groningen KVI cyclotron to energies of 10.8, 14.7, 19.2 MeV/nucleon. A heavy-residue counter consisting of a time-of-flight system and a ΔE - E telescope was placed at forward angles for the identification of the ER's. In this way, mass, charge, and energy of heavy ions, typically with masses up to 40 and energies down to 1 MeV/nucleon, can be measured simultaneously at three angles.⁵ In the 10.8- and 19.2-MeV/nucleon experiment 5°, 6°, and 7° were chosen, whereas at 14.7 MeV/nucleon these angles were 4.8°, 6°, and 7.2°. Three silicon-detector telescopes were placed on the opposite side of the beam at angles between 10° and 60° for the detection of α -particles. Energy spectra of α -particles correlated with ER's ($Z \geq 13$) are given in Fig. 1 for a projectile energy of 14.7 MeV/nucleon (filled circles).

A good description of the energy spectra at 40° and 60° is obtained with an evaporation model (dashed histograms, which will be discussed below), but at 10° an additional high-energy component due to preequilibrium emis-

sion is observed (solid line). In the coincident ER yield this ICF component was enhanced with respect to the CF component by selecting only events in which the velocity of the α -particles was greater than $v_\alpha \geq 0.87v_{\text{beam}}$. The mass distributions of ER's coincident with the fast α -particles are presented in Fig. 2 for the three beam energies (filled circles). The shaded area indicates the low-mass region where the ER velocity distribution broadens due to the contamination of mainly deep-inelastic collisions (DIC); the contributions from fission can be neglected for the present beam energies.

At beam energies in the range between 10 and 20

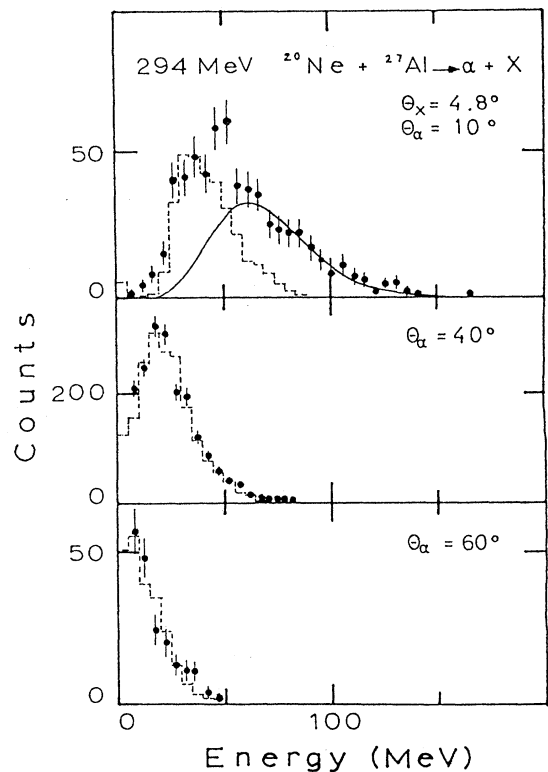


FIG. 1. Energy spectra of α -particles (filled circles) in coincidence with heavy residues ($Z \geq 13$) at 14.7 MeV/nucleon. The solid and dashed curves are results of calculations (see text).

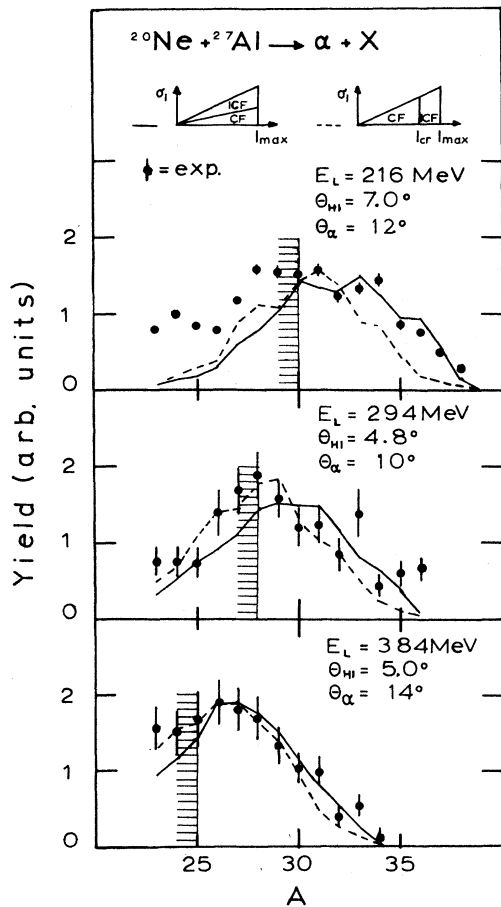


FIG. 2. Mass distributions of heavy residues in coincidence with preequilibrium α -particles. The two models for the localization in l space (see text and inset) are indicated by the dashed and solid curves.

MeV/nucleon breakup-fusion is the most likely reaction mechanism for preequilibrium α -emission.^{1,2,6,7} The energy distribution of fast light particles resulting from a breakup reaction can be described by a Fermi-gas model.^{1,2}

According to Murphy⁸ it can be written as

$$\frac{d^2\sigma}{dE d\Omega} = c\sqrt{E} \exp[-m(E + E_b - 2\cos\theta\sqrt{EE_b})/\sigma^2], \quad (1)$$

where the width is obtained from

$$\sigma^2 = \sigma_0^2 \frac{m(m_p - m)}{(m_p - 1)}. \quad (2)$$

In Eqs. (1) and (2), E is the energy of the particle in the laboratory frame, m its mass, θ the scattering angle, m_p the projectile mass, and E_b the energy of the particle traveling with beam velocity. The parameter σ_0 for ^{20}Ne is about 65 MeV/c.^{1,8}

Measurements of multiplicities¹ and Monte Carlo simulations (Fig. 3, see discussion in text) show that in ICF reactions approximately one α -particle is emitted pri-

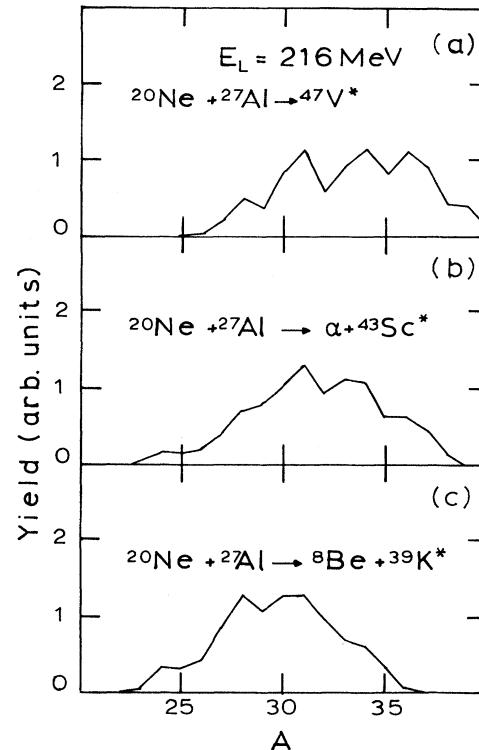


FIG. 3. The calculated heavy residue mass distribution at 10.8 MeV/nucleon for (a) complete fusion, (b) preequilibrium α -emission, and (c) preequilibrium ^8Be emission.

or to fusion. This was used in formulas 1 and 2 for the description of the high-energy component in the spectra of coincident α -particles at the three projectile energies (solid curve in Fig. 1). The restriction $v_\alpha \geq 0.87v_{\text{beam}}$ includes at least 87% of this breakup component and reduces contributions from statistical decay to at most 15%. Thus the coincidence requirement is in fact a good selection of the ICF process.

The impact-parameter range (or, equivalently, the range of angular momenta in the entrance channel) contributing to the ICF with α -particles produced in breakup-fusion reactions was studied by means of Monte Carlo simulations. The α -particle energy distribution was calculated with the Murphy model. Since the distribution is centered at the beam velocity, the preequilibrium emission of one α -particle moves on the average 20% of the total angular momentum in the entrance channel. Two extreme models for the range of contributing angular momenta in the entrance channel were considered. (1) CF occurs in an l window between $0\hbar$ and a critical value l_{cr} , whereas ICF is located between l_{cr} and l_{max} . (2) CF and ICF compete over the whole l window between $0\hbar$ and l_{max} . A schematic representation of these two models is included in the insets of Fig. 2. The total cross sections of CF and ICF were obtained from Morgenstern *et al.*⁴ and used to calculate l_{cr} and l_{max} . The values of $(l_{\text{cr}}, l_{\text{max}})$ at projectile energies of 10.8, 14.7, and 19.2 MeV/nucleon are (34,40), (33,44), and (29,47) in units of \hbar , respectively. At the present projectile energies precompound multi-

plicities are low¹ and thus the statistical model can be used to describe the decay process. The decay of the nucleus was simulated with a Monte Carlo version of the statistical model code PACE.⁹

For highly excited nuclei the influence of the shell structure vanishes and the parameters in the level density can be derived from the liquid-drop model.¹⁰ Standard values were chosen for the other parameters in the code PACE.

The dashed histograms in Fig. 1 are calculations of the statistical decay with model 2, scaled to the low-energy part of the experimental spectra. The coincident ER mass distributions were calculated for the models 1 and 2 and scaled to the experimental data in the region where DIC can be neglected (right of the shaded area). The interpretation is based on the shapes of the ER distributions, because the absolute coincident mass distribution strongly depends on the (unknown) angular distribution of the fast α -particles. The calculations include the effects of the energy distribution of the preequilibrium α -particles by running PACE for a distribution of initial excitation energies. ER's from DIC are not taken into account and thus the calculations underestimate the experimental yield for the lowest masses. The mass distributions calculated with model 2 (solid curve) are preferred to those of model 1 (dashed curve). Model 1 underestimates the mass integrated yield of ICF reactions at 10.8, 14.7, and 19.2 MeV/nucleon by 31, 25, and 15%, respectively, for masses above the shaded area. The shape of the mass yield is also better reproduced by model 2. A measure for the deviation of the Monte Carlo yield $F_{th}(A)$ from the experimental yield $F_{exp}(A)$ is the quantity:

$$\Delta^2 = \sum_A [F_{th}(A) - F_{exp}(A)]^2 / \sigma^2(A), \quad (3)$$

where $\sigma(A)$ is the experimental error and the sum is confined to the mass region where DIC can be neglected. For beam energies of 10.8, 14.7, and 19.2 MeV/nucleon model 1 gives values of Δ^2 , which exceed the values of model 2 by a factor of 7.6, 1.6, and 2.4, respectively. One should notice that the ratio ICF/CF grows with increasing

beam energy; therefore, the l -windows in the two models become more and more similar. A similar conclusion on the competition of ICF and CF was drawn from the analysis of the singles HR velocity spectra for the $^{16}\text{O} + ^{27}\text{Al}$ system at 9.4 MeV/nucleon.⁶

The calculations indicate a change of the ER yield with the number of α -particles emitted in the breakup process and thus the experimental yields reflect the multiplicity of fast α -particles. This is illustrated in Fig. 3, where inclusive ER mass distributions are shown for CF [Fig. 3(a)] and ICF with preequilibrium emission of either an α -particle [Fig. 3(b)] or ^8Be [Fig. 3(c)]. This latter process is experimentally equivalent to the preequilibrium emission of two α -particles. The calculations were performed at a projectile energy of 10.8 MeV/nucleon with the l -windows of model 2. Figure 3 shows that the ER mass distribution shifts towards lower masses as the mass of the spectator fragment increases. This trend is also found at projectile energies of 14.7 and 19.2 MeV/nucleon. Figure 3(c) fails to describe the experimental ER mass distribution of Fig. 2 (even if one includes the bias from the coincidence requirement) and consequently the preequilibrium emission of ^8Be is of minor importance.

In conclusion, the breakup-fusion model of ICF in combination with the statistical model of compound nucleus decay is able to give a good description of the ER mass distributions. Most of the ER's, measured in coincidence with an α -particle, are produced in breakup-fusion reactions in which the ^{20}Ne projectile breaks up in a ^{16}O and an α -particle. Most important, the ICF and CF processes compete over a wide range of impact parameters in the entrance channel.

We would like to thank the Kernfysisch Versneller Instituut, Groningen, The Netherlands for providing us with the heavy-ion beams. This work has been performed as part of the research program of the Stichting voor Fundamenteel Onderzoek der Materie (FOM) with financial support from the Nederlandse Organisatie voor Wetenschappelijk Onderzoek (NWO).

*On leave from the University of Warsaw, Warsaw, Poland.

†Present address: University of Pennsylvania, Philadelphia, PA 19104-6390.

‡Present address: Gesellschaft für Schwerionenforschung, Darmstadt 1, Germany.

¹K. Griffioen *et al.*, Phys. Rev. C **37**, 2502 (1988).

²C. Gregoire and B. Tamain, Ann. Phys. (Paris) **11**, 323 (1986).

³H. Morgenstern *et al.*, Phys. Lett. **113B**, 462 (1982).

⁴H. Morgenstern *et al.*, Z. Phys. A **313**, 39 (1983).

⁵E. A. Bakum, A. van den Brink, R. J. Meijer, and R. Kamermans, Nucl. Instrum. Methods Phys. Res. Sect. A **243**, 435 (1986).

⁶H. Ikezoe *et al.*, Nucl. Phys. A **444**, 349 (1985).

⁷H. Ikezoe *et al.*, Nucl. Phys. A **462**, 150 (1987).

⁸H. J. Murphy, Phys. Lett. **135**, 25 (1984).

⁹A. Gavron, Phys. Rev. C **21**, 230 (1980).

¹⁰F. Pühlhofer, Nucl. Phys. A **280**, 267 (1977).